STABILITY OF ELASTOMERIC SEISMIC ISOLATION BEARINGS

By Satish Nagarajaiah,[1] Member, ASCE, and Keith Ferrell,[2] Associate Member, ASCE

ABSTRACT: Elastomeric seismic isolation bearings are subjected to large axial loads and lateral displacements during strong earthquakes. The existing Koh-Kelly model for elastomeric bearings accounts for axial load effects on horizontal stiffness. This linear model is based on small displacements and rotations and predicts stable postcritical behavior or increasing critical load with increasing horizontal displacement; however, unstable postcritical behavior is observed in the bearing test results presented in this study. The analytical model developed in this study, based on the Koh-Kelly model, includes large displacements, large rotations, and nonlinearity of rubber, and it predicts unstable postcritical behavior. The formulation of the analytical model, calibration, and verification using experimental results are presented. It is shown that: (1) the critical load reduces with increasing horizontal displacement; and (2) the horizontal stiffness reduces with increasing horizontal displacement and axial load. It is also shown that the critical load capacity at a horizontal displacement equal to the width of the bearing is not equal to zero, as predicted by the approximate procedure used in design, but higher.

INTRODUCTION

The lateral flexibility of elastomeric seismic isolation bearings leads to a fundamental period of the base isolated structure that is much longer than both its fixed-base period and the predominant periods of the ground motion. The base shear and the superstructure displacements are reduced, due to this period shift, during strong earthquakes. However, large lateral displacements occur at the isolation level due to the flexibility of the bearings. The large lateral displacements and axial loads on the bearings influence: (1) the critical load of bearings; (2) the horizontal stiffness; (3) the bearing damping; (4) the bearing height; and (5) the bearing overturning (if the bearings are doweled). Hence, the stability of elastomeric bearings needs to be considered carefully during the analysis and design of the isolation system.

Early studies by Gent (1964) and Derham and Thomas (1981) were based on Haringx's theory (1948, 1949a and b); the decrease in horizontal stiffness with increasing axial load was predicted in both of these studies. Simo and Kelly (1984) used finite-element modeling to study the variation of lateral load-displacement behavior under increasing axial load. Stanton et al. (1990) and Roeder et al. (1987) studied the stability of laminated elastomeric bearings experimentally and theoretically with due consideration given to axial shortening. Buckle and Kelly (1986) studied the stability of elastomeric bearings using a model bridge deck tested using a shaking table. Bearing overturning or rollover was evident in these tests, since the bearings were doweled. Koh and Kelly (1986, 1988, 1989) developed a viscoelastic stability model and a mechanical model based on bearing test results.

The theoretical approach for the stability of rubber bearings has been to make use of Haringx's theory (1948, 1949a and b) based on linearity and small displacements. However, elastomeric bearings experience large displacements. Currently, this is accounted for approximately by reducing the value of critical load, P_{cro}, using the ratio of the effective column area and the actual column area at a large horizontal displacement (Buckle and Liu 1993):

$$P_{cr} = P_{cro}\left[1 - \frac{\Delta}{B}\right] \tag{1}$$

where P_{cr} = critical load; P_{cro} = critical load given by Haringx's theory; Δ = shear displacement; and B = bearing width. The dependence of horizontal stiffness on axial load is approximated (Buckle and Kelly 1986) by

$$K_h^* = K_h\left[1 - \left(\frac{P}{P_{cr}}\right)^2\right] \tag{2}$$

where P = axial load; K_h = stiffness at zero axial load; and K_h^* = modified stiffness.

Koh and Kelly (1986, 1988) have developed a model (a linear form of the nonlinear model shown in Fig. 1) that accounts for the influence of axial load on the horizontal stiffness of elastomeric bearings. Another paper by Koh and Kelly (1989) describes a viscoelastic model. Koh and Kelly (1986) compare the analytical results to experimental results. The experiments were performed under displacement control with harmonic motion of different amplitudes and constant axial load. Since the model is linear, the shear spring and rotational spring stiffnesses are constant. The actual stiffness of the bearings is nonlinear and displacement dependent (Koh and Kelly 1986). Hence, they adjust the shear spring stiffness and the

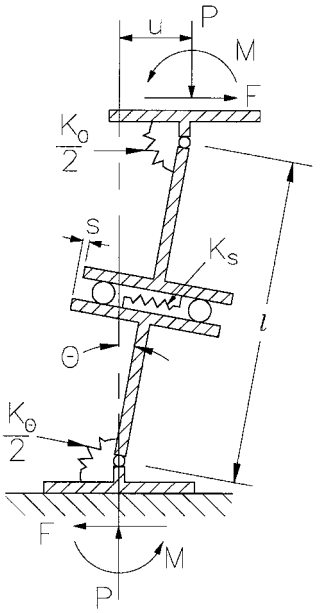

FIG. 1. Nonlinear Analytical Model Developed Based on Koh-Kelly Linear Model (K_s = Nonlinear Shear Stiffness; K_θ = Nonlinear Rotational Stiffness)

[1]Assoc. Prof., Dept. of Civ. Engrg., Rice Univ., 6100 Main St., Houston, TX 77005.

[2]Engr., Dept. of Transp., Jefferson City, MO 65102; formerly, Grad. Student, Dept. of Civ. Engrg., Univ. of Missouri, Columbia, MO 65211.

Note. Associate Editor: Sashi K. Kunnath. Discussion open until February 1, 2000. To extend the closing date one month, a written request must be filed with the ASCE Manager of Journals. The manuscript for this paper was submitted for review and possible publication on April 14, 1997. This paper is part of the ***Journal of Structural Engineering***, Vol. 125, No. 9, September, 1999. ©ASCE, ISSN 0733-9445/99/0009-0946–0954/$8.00 + $.50 per page. Paper No. 15573.

rotational spring stiffness of the linear model to match the nonlinear stiffness obtained from tests at a particular amplitude and obtain the horizontal stiffness variation, height reduction, and damping variation as a function of axial load. The theoretical results match the experimental results closely. The Koh-Kelly (1986, 1988) linear model predicts stable postbuckling behavior or increasing critical load with increasing horizontal displacement. However, the actual postbuckling behavior is unstable, as shown from the results of this study.

Experimental results (Buckle and Liu 1994; Buckle et al. 1999) show that the critical load, P_{cr}, decreases with increasing horizontal displacement; however, critical load does not decrease linearly with displacement, as predicted by (1). Experimental results (Buckle et al. 1999) also show that the shear force goes through a maximum as horizontal displacement increases, under constant axial load, and the shear force-displacement behavior is a function of axial load. Hence, the nonlinear horizontal tangential stiffness, K_h, is dependent on both horizontal displacement and axial load. P_{cr} and K_h, as functions of horizontal displacement, are not predicted accurately by Haringx's theory, the formula in (1) and (2), or the Koh-Kelly model (1986, 1989).

A nonlinear analytical model is developed in this study, based on the Koh-Kelly (1986) linear model, with the objective of predicting P_{cr} and K_h more accurately. The analytical model is verified using experimental results of Buckle et al. (1999).

BEARINGS TESTED

The multilayer elastomeric bearings tested by Buckle et al. (1999) consist of natural rubber layers and steel shims, as shown in Fig. 2. Thin rubber layers are bonded to the steel shims in alternating layers to produce the vertically stiff and horizontally flexible bearing. The alternating steel and rubber layers act to restrain the rubber layer from bulging laterally. All bearings tested had bolted connections at the top and bottom; hence, overturning was not a consideration.

A total of twelve bearings were tested. Nine of the square bearings tested were 5 in. × 5 in. (127 mm × 127 mm) in plan. Three of the square bearings tested were 10 in. × 10 in. (254 mm × 254 mm) in plan. Both the 5 in. and the 10 in. bearing properties are shown in Table 1 and Fig. 2; the 10 in. bearing properties are given in parentheses. The rubber layer thickness was varied to test bearings with different shape factors. The shape factor, S, is defined as

$$S = \frac{\text{loaded area of rubber layer}}{\text{force-free area of rubber layer}} \tag{3}$$

The steel shim thickness was varied to maintain the same height. The rubber cover was 1/8 in. (3.18 mm) for all bearings. All bearings tested had 1 in. (25.4 mm) thick end plates.

The rubber layer thickness in elastomeric bearings is typically less than 1/2 in. (12.7 mm); however, four of the bearing series tested (100, 200, 400, and 500) had rubber layer thicknesses greater than or equal to 1/2 in. (12.7 mm) to study the effect of low shape factor or increased slenderness. The 300

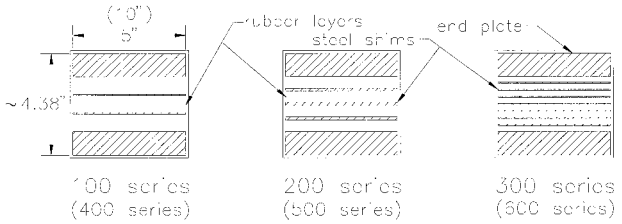

FIG. 2. Details of 5 and 10 in. Elastomeric Bearings Tested [Details in Parentheses for 10 in. Bearings (1.0 in. = 25.4 mm)]

TABLE 1. Five and Ten Inch Elastomeric Bearing Details (1 in. = 2.54 mm)

Bearings tested (1)	Nominal size $B \times B' \times H$[a] (in. × in. × in) (2)	Number of rubber layers (3)	Thickness of rubber layers (in.) (4)	Thickness of steel shim (in.) (5)	Shape factor (6)
101, 102, 103	5 × 5 × 4.375	3	0.75	0.0625	1.67
201, 202, 203	5 × 5 × 4.375	4	0.50	0.1250	2.50
301, 302, 303	5 × 5 × 4.385	8	0.25	0.0550	5.00
401	10 × 10 × 4.375	3	0.75	0.0625	3.33
501	10 × 10 × 4.375	4	0.50	0.1250	5.00
601	10 × 10 × 4.385	8	0.25	0.0550	10.00

[a]B = width of square bearing; B' = breadth; H = height of bearing.

series and 600 series of bearings had 1/4 in. (6.35 mm) rubber layer thicknesses.

The elastomeric bearings were tested using the uniaxial single bearing test rig at the Earthquake Engineering Research Center at the University of California at Berkeley. The test rig apparatus consisted of a vertical loading mechanism and a horizontal loading mechanism. The vertical load was generated by the two vertical actuators on either side of the bearing. The horizontal actuator provided the lateral force to displace the bearing to the desired displacement. The bearings were tested for stability individually under quasi-static conditions.

Since the 300 series bearings are more typical, the test results of one of the bearings in the series, i.e., bearing 302, is presented in detail, and the test results of the other series (100, 200, 400, 500, and 600 series) are presented briefly. The complete details of the test procedure and test results for the 100, 200, 300, 400, 500, and 600 series can be found in Buckle et al. (1999).

TEST RESULTS

The shear force–horizontal displacement, F-u, curves are shown in Fig. 3 as a function of axial load for bearing 302. Two important features to be noted in Fig. 3 are as follows: (1) the F-u curves go through a maximum as the horizontal displacement increases, under constant axial load; and (2) the shear force and horizontal displacement at which the maximum occurs decrease with increasing axial load. The severe nonlinearities are clearly evident in Fig. 3.

The axial load–horizontal displacement, P-u, variation is shown in Fig. 4 as a function of shear force for bearing 302.

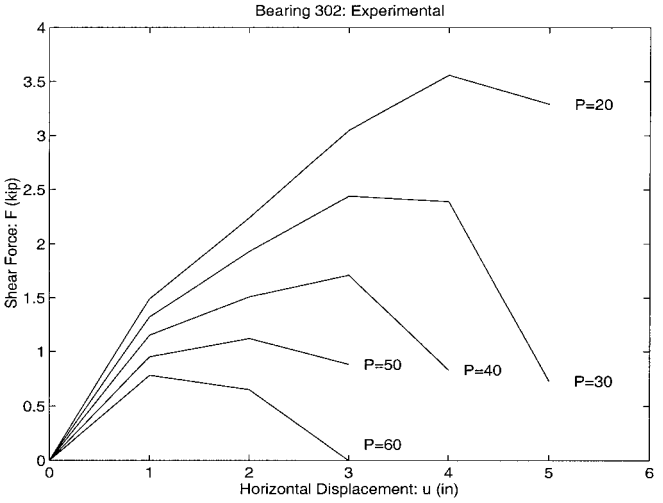

FIG. 3. Stability Test: Shear Force–Displacement Curves as Function of Axial Load for Bearing 302 of Width B = 5 in., with Shape Factor S = 5 (1 kip = 4.45 kN; 1 in. = 25.4 mm)

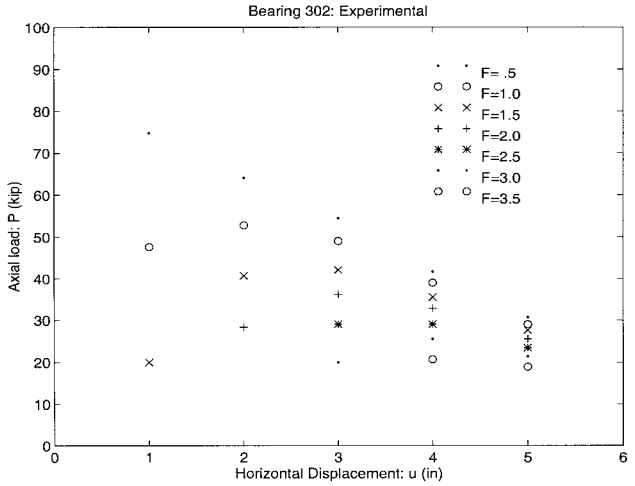

FIG. 4. Stability Test: Axial Load–Horizontal Displacement Variation as Function of Shear Force for Bearing 302 with *B* = 5 in., *S* = 5

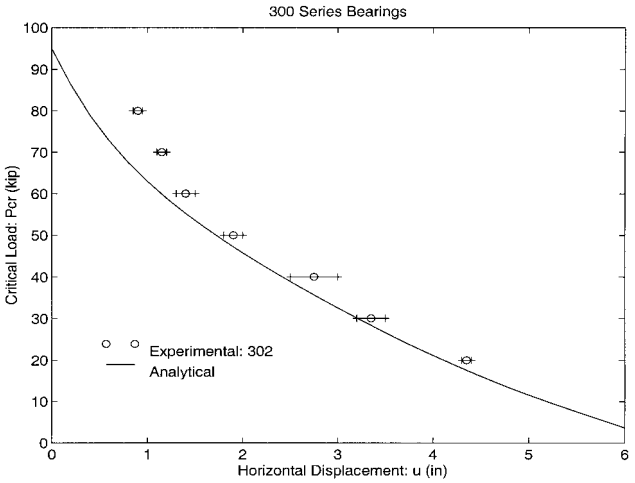

FIG. 5. Variation of Critical Load with Horizontal Displacement of 300 Series Bearings with *B* = 5 in., *S* = 5

The equilibrium path, a smooth curve passing through discrete points, shown in Fig. 4, at each shear force level, goes through a limit point, which is the critical load. The equilibrium paths are unstable past the limit point in Fig. 4; hence the critical load decreases with increasing horizontal displacement. The critical load, P_{cr}, obtained from Fig. 4 is shown in Fig. 5 as a function of horizontal displacement. The shear force–horizontal displacement curves in Fig. 3 can be used to verify the critical load, because at P_{cr} the horizontal tangential stiffness goes to zero.

In Fig. 5 it is evident that significant reduction in P_{cr} occurs at horizontal displacements equal to the width of the bearing, B = 5 in. The error bars in Fig. 5 represent the variability of the recovered test results, since the tests were performed only at 1, 2, 3, 4, and 5 in. horizontal displacements and the points in between these displacements were recovered by curve fitting techniques.

The observed reduction in P_{cr} cannot be predicted using the Koh-Kelly model because it is based on linearity and small displacements. In view of this, a nonlinear analytical model is developed.

NONLINEAR ANALYTICAL MODEL

The nonlinear analytical model developed in this study, shown in Fig. 1, is based on the Koh and Kelly (1986) linear model. The key developments in this study are that the shear and rotational springs are considered to be nonlinear elastic and that large displacements and rotations are considered. The nonlinearities are based on the test results. The natural rubber bearings considered in this study do not have significant path dependent behavior. In view of this, the nonlinear elastic springs are deemed to be adequate. The inclusion of the path dependent behavior in the model and the appropriate tests needed for the verification of such a model are the subjects of a future study.

The developed nonlinear analytical model has two rigid elements of total height l in the shape of tees connected at midheight by a shear spring and frictionless rollers and connected to the top and bottom plate by moment springs and frictionless hinges. The model has two degrees of freedom (DOF). The shear DOF, s, is due to frictionless rollers and is resisted by a nonlinear shear spring of stiffness K_s. The rotational DOF, θ, is due to frictionless hinges and is resisted by nonlinear rotational springs of stiffness $K_\theta/2$, where K_θ = rotational stiffness or tilting stiffness. The model is loaded by axial load P and horizontal load F at the top of the column. The top plate is free to move in the vertical and horizontal directions; however, it is restrained in the rotational direction. The horizontal displacement, u, of the top of the column is

$$u = l \sin\theta + s \cos\theta \tag{4}$$

The nonlinear horizontal stiffness of the model, K_h, is a function of the shear force, F, and the horizontal displacement, u. In the nonlinear analytical model developed, both the shear stiffness, K_s, and the rotational stiffness, K_θ, vary as a function of the shear deformation, s.

Equilibrium Equations

The equilibrium equations for the model shown in Fig. 1 with the nonlinear shear stiffness and rotational stiffness springs are given by:

- Shear equilibrium:

$$K_{so}\left(1 - C_s f\left(\frac{s}{l_r}\right)\right) s = F\cos\theta + P\sin\theta + \frac{K_{\theta o} C_\theta \theta^2}{2} \tag{5}$$

- Rotational equilibrium:

$$K_{\theta o}\left(1 - C_\theta\left(\frac{s}{l_r}\right)\right)\theta = P(l\sin\theta + s\cos\theta) + F(l\cos\theta - s\sin\theta) \tag{6}$$

where C_s and C_θ = constants; $f(s/l_r)$ is a function of s and l_r, the total thickness of all rubber layers; l = combined height of the rubber layers and steel plates, excluding the top and bottom steel plates; and K_{so} and $K_{\theta o}$ = shear stiffness and rotational stiffness, respectively, at zero shear strain.

The height reduction, h, can be computed using the following equation:

$$h = l(1 - \cos\theta) + s\sin\theta \tag{7}$$

Eqs. (5) and (6), a nonlinear system of equations, are solved numerically in the incremental form.

If nonlinear terms such as $C_s f(s/l_r)$, $C_\theta s/l_r$, θ^2, and $s\theta$ are neglected, and the terms $\sin\theta$ and $\cos\theta$ are replaced by θ and 1, respectively, for small angles, the nonlinear model reduces to the Koh-Kelly model (1986), resulting in the following equations:

$$u = l\theta + s; \quad K_{\theta o}\theta = P(l\theta + s) + Fl; \quad K_{so}s = P\theta + F \tag{8a–c}$$

Solving for θ and s yields

$$\theta = \frac{(K_{so}l + P)F}{\left(\frac{K_{\theta o}}{l} - P\right)(K_{so}l) - P^2} \tag{9a}$$

$$s = \frac{K_{\theta o}F}{\left(\frac{K_{\theta o}}{l} - P\right)(K_{so}l) - P^2} \tag{9b}$$

The critical load can be determined by setting the denominator of the expressions for θ and $s = 0$:

$$P_{cr} = \frac{-K_{so}l \pm \sqrt{K_{so}^2 l^2 + 4K_{\theta o}K_{so}}}{2} \tag{10}$$

To obtain relations for $K_{\theta o}$ and K_{so} in terms of the bearing properties: (1) neglect the shear deformation by letting K_{so} tend toward infinity to get $K_{\theta o}$; and (2) neglect flexural deformations by letting $K_{\theta o}$ tend toward infinity to get K_{so}:

$$K_{\theta o} = P_E l; \quad K_{so} = \frac{(GA_s)_{\text{eff}}}{l} = \frac{P_s}{l} \tag{11a}$$

where

$$P_E = \frac{\pi^2 (EI)_{\text{eff}}}{l^2}; \quad P_s = (GA_s)_{\text{eff}} \tag{11b}$$

P_{cr} is obtained by substituting $K_{\theta o}$ and K_{so} in (10) and considering the positive solution:

$$P_{cr} = \frac{(GA_s)_{\text{eff}}}{2}\left[\sqrt{1 + 4\frac{P_E}{(GA_s)_{\text{eff}}}} - 1\right] \tag{12}$$

where $(GA_s)_{\text{eff}}$ = effective shear rigidity; and $(EI)_{\text{eff}}$ = effective flexural rigidity. P_{cr} is identical to the critical load given by Haringx's theory (1948, 1949a and b). The horizontal stiffness, K_{ho}, is given by

$$K_{ho} = \frac{F}{u}; \quad u = l\theta + s \tag{13a}$$

$$K_{ho} = \frac{F}{u} = \frac{P_s}{l}\left(\frac{1 - \frac{P}{P_E} - \frac{P^2}{P_E P_s}}{1 + \frac{P}{P_E} + \frac{P_s}{P_E}}\right) \tag{13b}$$

and the height reduction:

$$h = \frac{l\theta^2}{2} + s\theta \tag{14}$$

The horizontal stiffness, K_{ho}, can be approximated by the following expression:

$$K_{ho} = \frac{P_s}{l}\left(1 - \frac{P^2}{P_E P_s}\right) \tag{15}$$

Parameters

The elastomer properties were not available. Even when they are available, the elastomer used in the bearing may have somewhat different properties than the elastomer used in tests pertaining to data sheets. It has been observed in past experiments that the bearings usually have different properties than the small elastomer specimen used to determine basic properties (Koh and Kelly 1986). In view of this, an indirect approach, similar to the one used by Koh and Kelly (1986), was adopted to estimate the value of the shear modulus, G. The horizontal tangential stiffness, K_h, as a function of displacement was estimated from the quasi-static tests on bearing 302. The shear modulus, G, was estimated from (15). The estimated G was 0.2 ksi for 0% shear strain and 0.136 ksi for 100% shear strain. The variation of G was estimated from the variation of K_h:

$$G = G_o\left(1 - C_s \tanh\left(\alpha\frac{u}{l_r}\right)\right) \tag{16}$$

where G_o = 0.2 ksi; C_s = dimensionless constant = 0.325; and α = dimensionless constant with a value of l_r. The following relations (Buckle and Kelly 1986; Koh and Kelly 1986) were used to establish the effective shear rigidity and effective flexural rigidity:

$$(GA_s)_{\text{eff}} = GA\frac{l}{l_r} \tag{17}$$

$$(EI)_{\text{eff}} = E_r I\frac{l}{l_r} \tag{18}$$

where l = combined height of the rubber layers and steel plates, excluding the top and bottom plates; l_r = total thickness of all rubber layers; I = moment of inertia of the bearing about the axis of bending; and

$$E_r = E_o(1 + 0.742S^2) \tag{19}$$

where E_o = elastic modulus of rubber = $4G$.

The variation of nonlinear shear stiffness, K_s, as a function of shear deformation, s, was assumed to be similar to the estimated variation of G as a function of horizontal displacement:

$$K_s = K_{so}\left(1 - C_s \tanh\left(\alpha\frac{s}{l_r}\right)\right) \tag{20}$$

where C_s = dimensionless constant = 0.325; K_{so} = shear spring stiffness at zero strain from (11); and α = dimensionless constant with a value of l_r. The variation of nonlinear rotational stiffness, K_θ, which yields the appropriate unstable postcritical behavior as well as the correct behavior of critical load and shear force as a function of horizontal displacement, is as follows:

$$K_\theta = K_{\theta o}\left(1 - C_\theta\frac{s}{l_r}\right) \tag{21}$$

where $K_{\theta o}$ = rotational spring stiffness at zero strain from (11); C_θ = dimensionless constant = $C'_\theta\alpha$; and C'_θ = dimensionless constant. The variation of nonlinear rotational stiffness, K_θ, when considered as a decreasing function of θ—as one would expect—led to acceptable shear force–horizontal displacement, F-u, behavior. However, it also led to incorrect axial load–horizontal displacement, P-u, behavior in the postcritical range, inconsistent with the test results. Also, the variation of K_θ based on moment-rotational curves could not be established consistently for all bearings from test results. Due to such inconsistencies, K_θ as a function of s/l_r in (21) was adopted. Since both s and θ are internal variables, this was deemed admissible. The reduction factor C'_θ, which determines the drop in rotational stiffness, was arrived at based on the experimental results of bearings 302 and 201. The physically motivated formula developed for C'_θ based on the rubber layer thickness/shape factor is as follows:

$$C'_\theta = \left(\frac{t_u}{B} - \frac{t_r}{B}\right) \tag{22}$$

where t_u = rubber layer of unit thickness; t_r = rubber layer thickness; and B = width of the bearing. For a square bearing with shape factor $S = B/(4t_r)$:

$$C'_\theta = \frac{1}{4}\left(\frac{1}{S_u} - \frac{1}{S}\right) \tag{23}$$

where S_u = shape factor of rubber layer of unit thickness; and S = shape factor of the rubber layer. For a bearing with very large S, $t_r \approx 0$, with B = 5 in. and S_u = 1.25, C'_θ = 0.2. For a bearing $S = S_u$, t_r = 1 in., C'_θ = 0. For 300 series bearings, C'_θ = 0.15. Hence, C'_θ developed based on the shape factor of the bearing can be used for 5 in., 10 in., or other bearings, within limits of t_r not greater than the unit thickness and B not less than the unit length.

CALIBRATION OF ANALYTICAL MODEL USING EXPERIMENTAL RESULTS OF 300 AND 200 SERIES BEARINGS

The parameter C'_θ in (22) was calibrated using experimental results of bearings 302 and 201. The values K_{so} = 2.5 kip/in. and $K_{\theta o}$ = 4,016 kip/in. for 300 series bearings were obtained based on (11). Eqs. (5) and (6) were solved numerically. The comparison of analytical and experimental horizontal tangential stiffness, K_h, is shown in Fig. 6 for 300 series bearings. To illustrate the effect of having constant K_s and K_θ, as in the Koh-Kelly model, equilibrium paths for the case with spring stiffnesses set to K_{so} and $K_{\theta o}$ are shown in Fig. 7 for 300 series bearings. The equilibrium paths indicate stable postcritical behavior, as shown by Koh and Kelly (1988). The equilibrium paths for the nonlinear analytical model developed in this study for 300 series bearings are shown in Fig. 8. The equilibrium paths are unstable past the limit point, as observed in the experimental results. The critical load occurs at the limit point of each equilibrium path, and the horizontal tangential stiffness, K_h, is equal to zero at the limit point. Due to the unstable equilibrium paths, the critical load decreases with increasing horizontal displacement. The critical load–horizontal displacement, P_{cr}-u, curve from the analytical model for 300 series bearings and experimental results for bearing 302 is shown in Fig. 5. The analytical and experimental results are in good agreement.

The analytical shear force–horizontal displacement, F-u, curves for 300 series bearings are compared with test results for bearing 302 in Fig. 9 at different axial load levels. From Fig. 9 it is evident that the analytical model captures the nonlinear behavior and axial load effects accurately. Fig. 9 also shows the horizontal tangential stiffness variation with horizontal displacement and axial load. Note that the horizontal tangential stiffness, K_h, is zero at the displacement where the shear force–displacement curve is maximum. The horizontal stiffness decreases with increasing axial load and horizontal displacement.

Fig. 10 shows the horizontal tangential stiffness variation as a function of horizontal displacement and axial load. The K_h-P-u surface in Fig. 10 shows that the horizontal tangential stiffness, K_h, decreases with increasing axial load and horizontal displacement. The effects of the nonlinearities of the elastomeric bearing and the axial load are significant, as evident in Fig. 10. The effects of axial load and horizontal displacement on horizontal stiffness can alter the seismic response of base isolated structures (Nagarajaiah et al. 1991).

The height reduction due to horizontal displacement of the bearing, given by (7), as a function of axial load is shown in Fig. 11 for 300 series bearings. The experimental results for bearing 302, as shown in Fig. 11, do not include the vertical deformation due to axial flexibility of the bearing; this estimated deformation has been subtracted from the overall height reduction. This is necessary, as the new model does not include axial flexibility. Comparison between the analytical and experimental results indicates that useful estimates of the height reduction can be obtained.

The equilibrium paths for the 200 series bearings are shown in Fig. 12. The critical load–horizontal displacement, P_{cr}-u, curve from the analytical model for 200 series bearings and the experimental results of bearing 201 are shown in Fig. 13.

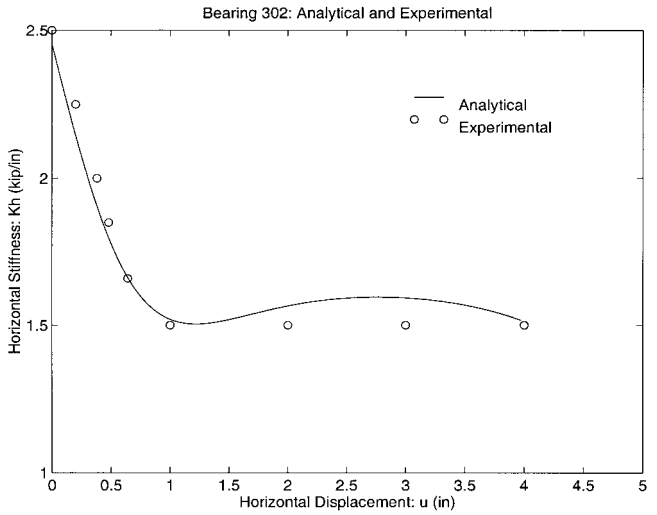

FIG. 6. Variation of Horizontal Tangential Stiffness with Horizontal Displacement of 300 Series Bearings with B = 5 in., S = 5

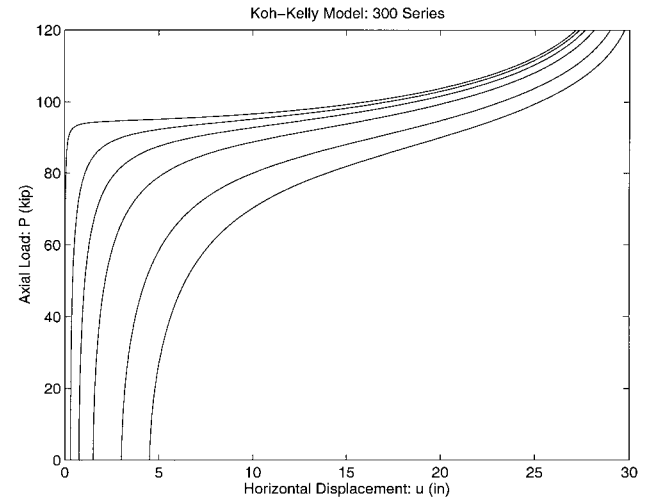

FIG. 7. Stable Equilibrium Paths of Axial Load–Horizontal Displacement Predicted by Koh-Kelly Model of 300 Series Bearings with B = 5 in., S = 5

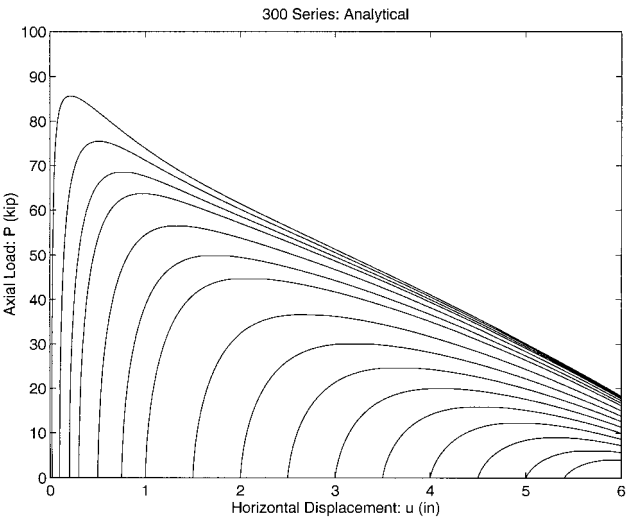

FIG. 8. Unstable Equilibrium Paths of Axial Load–Horizontal Displacement Predicted by Nonlinear Analytical Model of 300 Series Bearings with B = 5 in., S = 5; Critical Load Occurs at Limit Point of Each Equilibrium Path

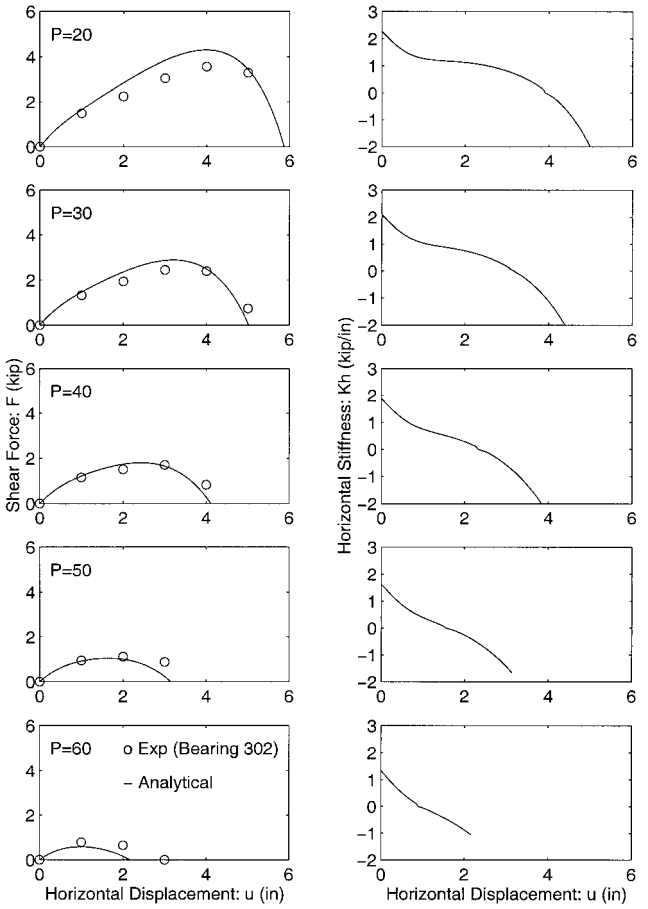

FIG. 9. Results for 300 Series Bearings with *B* = 5 in., *S* = 5; Shear Force–Horizontal Displacement Curves at Maximum when Horizontal Tangential Stiffness Curves Are at Zero

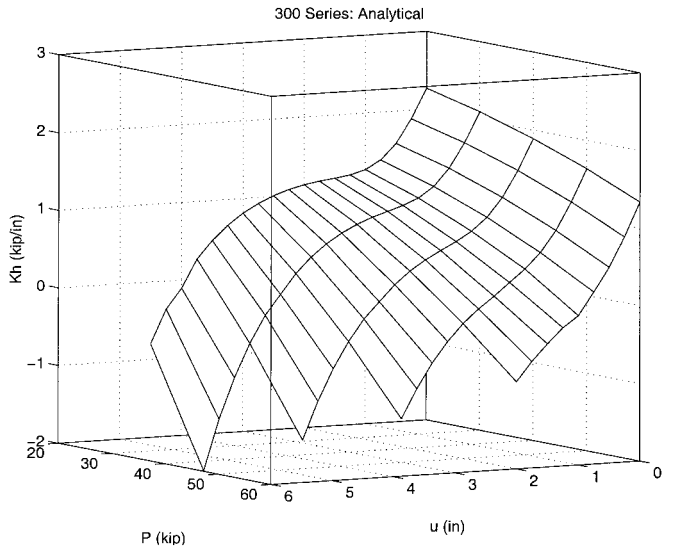

FIG. 10. Variation of Horizontal Tangential Stiffness, K_h, with Axial Load, *P*, and Horizontal Displacement, *u*, of 300 Series Bearings with *B* = 5 in., *S* = 5

The analytical and experimental results are in good agreement. The critical load drops with increasing horizontal displacement because the equilibrium paths are unstable. The critical load at a horizontal displacement equal to the width of the bearing (5 in.) is higher than the value of zero estimated by (1). The analytical shear force–horizontal displacement, *F*-*u*, curves

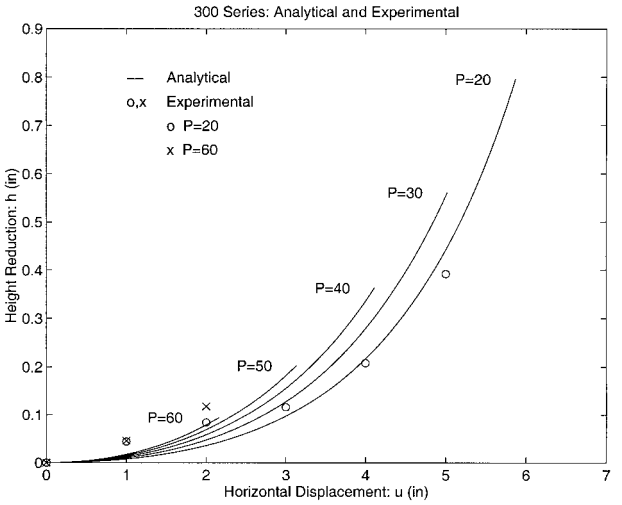

FIG. 11. Height Reduction due to Horizontal Displacement as Function of Axial Load for 300 Series Bearings with *B* = 5 in., *S* = 5

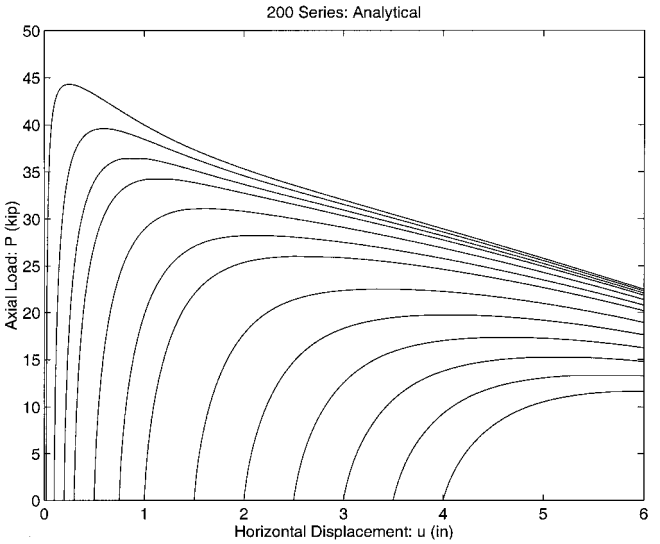

FIG. 12. Unstable Equilibrium Paths of Axial Load–Horizontal Displacement of 200 Series Bearings with *B* = 5 in., *S* = 2.5; Critical Load Occurs at Limit Point of Each Equilibrium Path

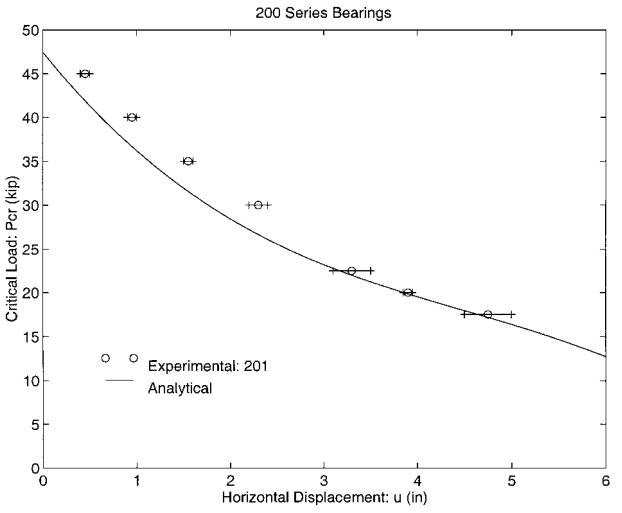

FIG. 13. Variation of Critical Load with Horizontal Displacement of 200 Series Bearings with *B* = 5 in., *S* = 2.5

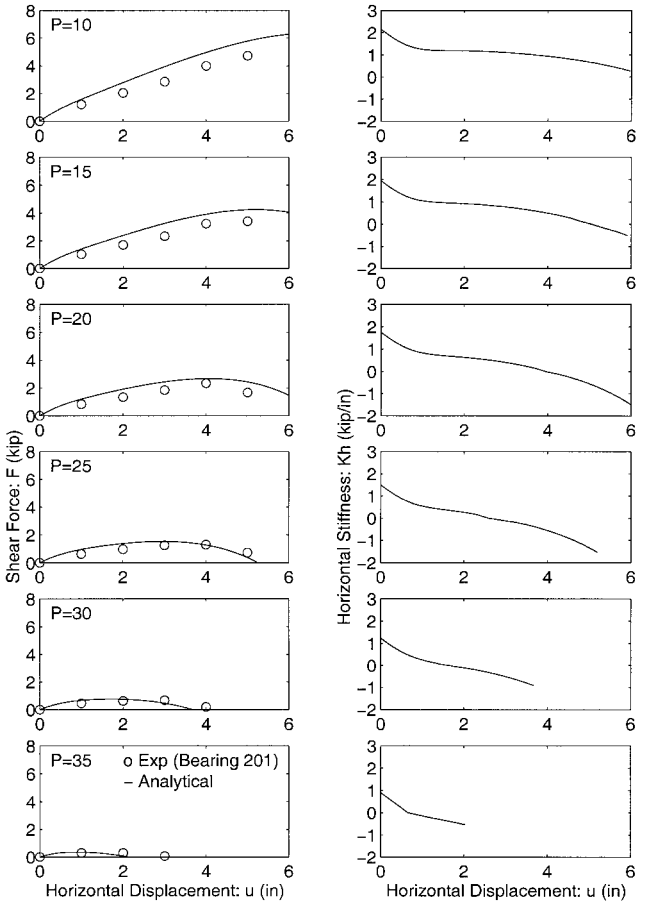

FIG. 14. Results for 200 Series Bearings with *B* = 5 in., *S* = 2.5; Shear Force–Horizontal Displacement Curves at Maximum when Horizontal Tangential Stiffness Curves Are at Zero

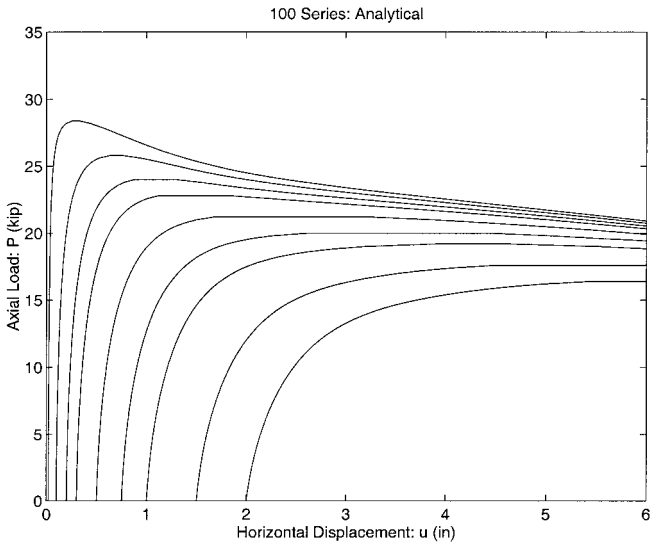

FIG. 15. Unstable Equilibrium Paths of Axial Load–Horizontal Displacement of 100 Series Bearings with *B* = 5 in., *S* = 1.67; Critical Load Occurs at Limit Point of Each Equilibrium Path

compared with test results for bearing 201 at different axial load levels, as shown in Fig. 14, indicate good agreement.

EXPERIMENTAL VERIFICATION OF ANALYTICAL MODEL

The model was verified using the test results of 100, 400, 500, and 600 series bearings, which were not used in the calibration of the model. The results of the verification are presented.

The equilibrium paths for the 100 series bearings are shown in Fig. 15. The critical load–horizontal displacement, P_{cr}-u, curve from the analytical model for 100 series bearings and the experimental results of bearing 103 are shown in Fig. 16. The P_{cr}-u curve and test results shown in Fig. 16 for bearing 103 indicate that the analytical results capture the trend in the experimental results satisfactorily; the differences between the experimental and analytical results can be partly attributed to variability in the recovered test data. It is also evident from

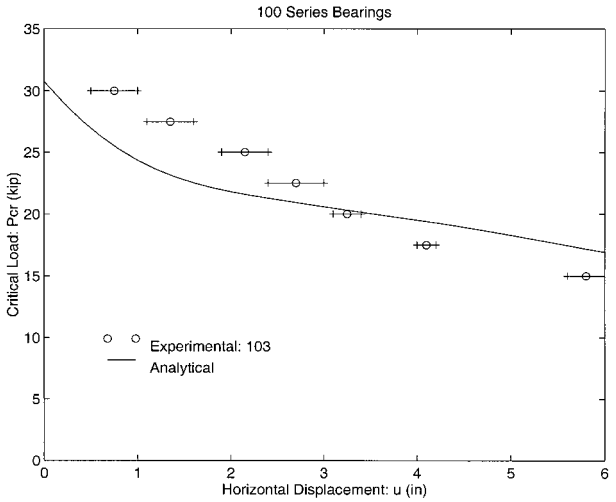

FIG. 16. Variation of Critical Load with Horizontal Displacement of 100 Series Bearings with *B* = 5 in., *S* = 1.67

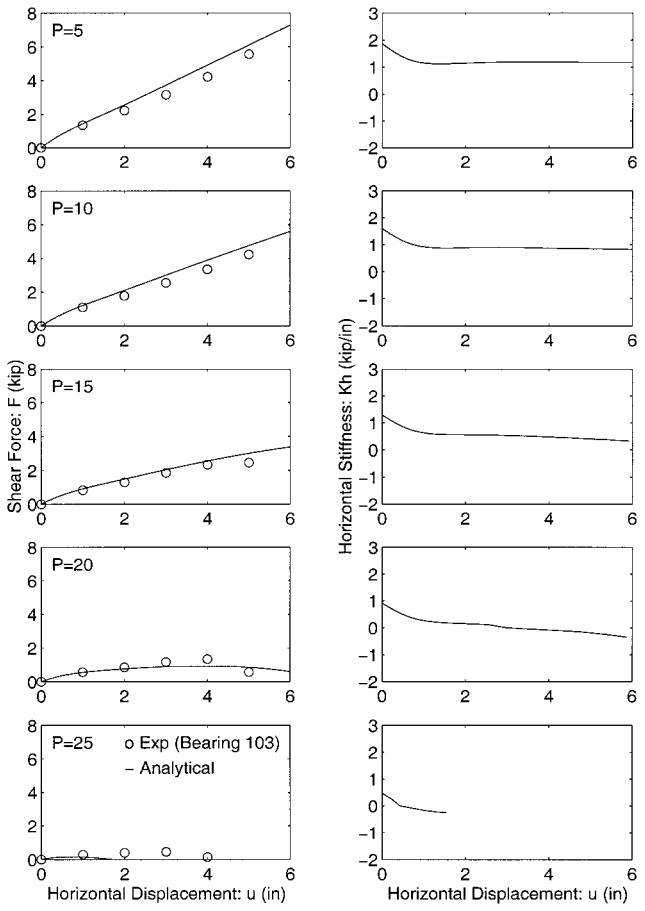

FIG. 17. Results for 100 Series Bearings with *B* = 5 in., *S* = 1.67; Shear Force–Horizontal Displacement Curves at Maximum when Horizontal Tangential Stiffness Curves Are at Zero

Fig. 16 that the drop in critical load as a function of horizontal displacement is not as significant as in 300 series bearings. Substantial critical load capacity exists at a displacement equal to the width of the bearing (5 in.) when compared with a value of zero obtained using (1). The comparison of analytical shear force–horizontal displacement, *F*-*u*, curves with test results for bearing 103 at different axial load levels, as shown in Fig. 17, is satisfactory.

The P_{cr}-*u* curves from test results for 401, 501, and 601 series bearings could not be obtained because the bearings were not loaded to such high levels of axial load due to test setup limitations. The analytical P_{cr}-*u* curves for 401, 501, and 601 series bearings are shown in Fig. 18. The P_{cr}-*u* curves based on the approximate formula in (1) are also shown. It is evident that critical load capacity exists at horizontal displacements equal to the width of the bearing (10 in.) when compared with the zero critical load predicted in (1). The approximate formula is not conservative at all horizontal displacements. A comparison between analytical and experimental shear force–horizontal displacement curves at low axial load levels is shown in Fig. 18 for bearings 401, 501, and 601. The comparison is satisfactory.

In a separate study (Buckle et al. 1999) nonlinear finite-element analysis results obtained for 200, 300, 500, and 600 series bearings compared favorably with the results of the analytical model developed in this study. Interested readers are referred to Buckle et al. (1999).

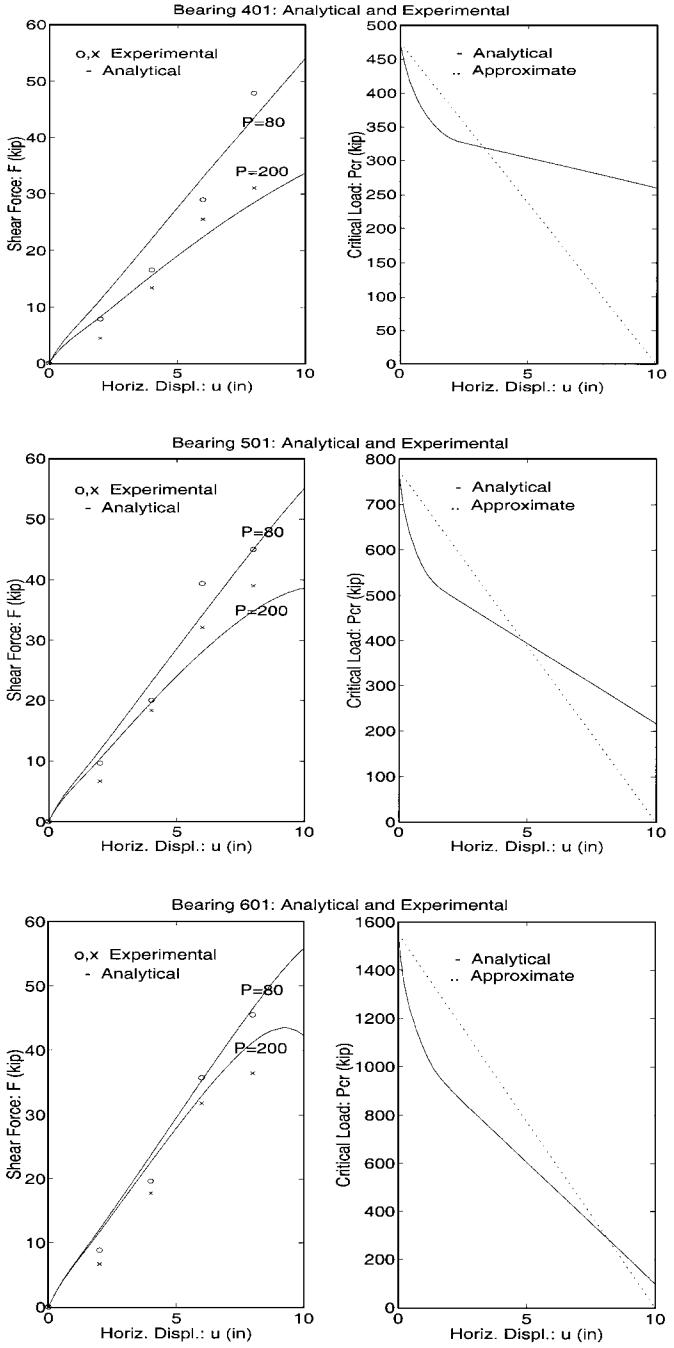

FIG. 18. Results for 10 in. Bearings 401 (*S* = 3.33), 501 (*S* = 5) and 601 (*S* = 10); Shear Force–Horizontal Displacement Curves and Critical Load–Horizontal Displacement Curves, Obtained from Experiments, Analytical Model, and Approximate Formula in Eq. (1)

CONCLUSIONS

A nonlinear analytical model has been developed based on the Koh-Kelly linear model. The model includes large displacements and rotations and nonlinearities in shear and rotational stiffness of the bearing. The model is capable of predicting the nonlinear and postcritical behavior of elastomeric bearings of different sizes and shape factors. The postcritical behavior is unstable, as evident from the test results. This behavior can be predicted only when the nonlinearities are fully accounted for. A linear model will predict stable postcritical behavior. The developed nonlinear model predicts the unstable postcritical behavior successfully.

The developed nonlinear analytical model satisfactorily predicts the behavior observed in the test results of the bearings, such as: (1) the reduction in critical load with increasing horizontal displacement; (2) the nonlinear shear force–horizontal displacement behavior as a function of axial load (the shear force–horizontal displacement curves go through a maximum as the horizontal displacement increases; the shear force and horizontal displacement at which the maximum occurs decrease with increasing axial load); (3) the horizontal stiffness variation, which decreases with increasing axial load and horizontal displacement; and (4) the height reduction due to increasing horizontal displacement.

Other important conclusions of this study are as follows. A higher critical load capacity exists at a horizontal displacement equal to the width of the bearing and is not equal to zero, as predicted by the approximate design formula. The approximate design formula is not conservative at all horizontal displacements. The reduction in critical load with increasing horizontal displacement depends on the reduction in shear stiffness and rotational stiffness as a function of shear displacement. The reduction in rotational stiffness depends on the shape factor and the rubber layer thickness of the bearing in comparison with a rubber layer of unit thickness. The calibration and verification of the analytical model is based on a limited set of test results; hence, further investigations are needed.

ACKNOWLEDGMENTS

The funding for this project provided by the Multidisciplinary Center for Earthquake Engineering Research and the National Science Foundation (Grant 94-5001B/955101) is gratefully acknowledged. The first writer is indebted to Professor Ian Buckle for his assistance and encouragement during the course of the project. Bearing tests were conducted under the guidance of Professors Ian Buckle and James Kelly at the Earthquake Engineering Research Center. The assistance of Dr. Peter Clark in recovering the raw test data is gratefully acknowledged.

APPENDIX. REFERENCES

Buckle, I. G., and Kelly, J. M. (1986). ''Properties of slender elastomeric isolation bearings during shake table studies of a large-scale model bridge deck.'' *Joint Sealing and bearing systems for concrete structures*, Vol. 1, American Concrete Institute, Detroit, Mich., 247–269.
Buckle, I. G., and Liu, H. (1993). ''Stability of elastomeric seismic iso-

lation systems.'' *Proc., Seminar on Seismic Isolation, Passive Energy Dissipation, and Control*, Applied Technology Council, Redwood City, Calif., 293–305.
Buckle, I. G., and Liu, H. (1994). ''Experimental determination of critical loads of elastomeric isolators at high shear strain.'' *NCEER Bull.*, 8(3), 1–5.
Buckle, I. G., Nagarajaiah, S., and Ferrell, K. (1999). ''Stability of elastomeric seismic isolation bearings: experimental study.'' *J. Struct. Engrg.*, ASCE, in review.
Derham, C. J., and Thomas, A. G. (1981). ''The design of seismic isolation bearings.'' *Control of seismic response of piping system and other structures*. University of California, Berkeley, Calif., 21–36.
Ferrell, K. (1996). ''Stability of elastomeric seismic isolation bearings,'' MS thesis, University of Missouri, Columbia.
Gent, A. N. (1964). ''Elastic stability of rubber compression springs.'' *J. Mech. Engrg. Sci.*, 6(4), 318–326.
Haringx, J. A. (1948). ''On highly compressible helical springs and rubber rods and their application for vibration-free mountings. I.'' *Philips Res. Rep.*, 3, 401–449.
Haringx, J. A. (1949a). ''On highly compressible helical springs and rubber rods and their application for vibration-free mountings. II.'' *Philips Res. Rep.*, 4, 49–80.
Haringx, J. A. (1949b). ''On highly compressible helical springs and rubber rods and their application for vibration-free mountings. III.'' *Philips Res. Rep.*, 4, 206–220.
Kelly, J. M. (1997). *Earthquake resistant design with rubber*, 2nd Ed., Springer Verlag, New York.
Koh, C. G., and Kelly, J. M. (1986). ''Effects of axial load on elastomeric bearings.'' *UCB/EERC-86/12*, Earthquake Engrg. Res. Ctr., University of California, Berkeley, Calif.
Koh, C. G., and Kelly, J. M. (1988). ''A simple mechanical model for elastomeric bearings used in base isolation.'' *Int. J. Mech. Sci.*, 30(12), 933–943.
Koh, C. G., and Kelly, J. M. (1989). ''Viscoelastic stability model for elastomeric isolation bearings.'' *J. Struct. Engrg.*, ASCE, 115(2), 285–302.
Nagarajaiah, S., Reinhorn, A. M., and Constantinou, M. C. (1991). ''3D-BASIS nonlinear dynamic analysis of three-dimensional base isolated structures. II.'' *Rep. NCEER-91-0005*, National Center for Earthquake Engineering Research, SUNY, Buffalo.
Roeder, C. W., Stanton, J. F., and Taylor, A. W. (1987). ''Performance of elastomeric bearings.'' *NCHRP Rep. 298*, Transp. Res. Board, National Research Council, Washington, D.C.
Simo, J. C., and Kelly, J. M. (1984). ''Finite element analysis of the stability of multilayer elastomeric bearings.'' *Engrg. Struct.*, 6, 162–174.
Stanton, J. F., Scroggins, G., Taylor, A. W., and Roeder, C. W. (1990). ''Stability of laminated elastomeric bearings.'' *J. Engrg. Mech.*, ASCE, 116(6), 1351–1371.